Inorg. Chem. **2006**, *45*, 3191–3202

Structural and Spectroscopic Characterization of Copper(II) Complexes of a New Bisamide Functionalized Imidazole Tripod and Evidence for the Formation of a Mononuclear End-On Cu–OOH Species

Lionel E. Cheruzel,[†] Matthew R. Cecil,[†] Sara E. Edison,[‡] Mark S. Mashuta,[†] Michael J. Baldwin,[‡] and Robert M. Buchanan*,[†]

Department of Chemistry, University of Louisville, Louisville, Kentucky 40292, and Department of Chemistry, University of Cincinnati, P.O. Box 210172, Cincinnati, Ohio 45221-0172

Received July 29, 2005

A new polyimidazole tripod *N*,*N*-bis((1-methyl-4-pivalamidoimidazol-2-yl)methyl)-*N*′-((1-methylimidazol-2-yl)methyl)-amine (**L2**) has been synthesized and shown to form intramolecular hydrogen bonds with different axial ligands bonded to Cu(II) in the solid state. The same hydrogen-bonding property of **L2** appears responsible for the stabilization of a Cu(II)–OOH species in solution. The crystal structures of **L2** and three of its Cu(II) complexes are reported. The [Cu(**L2**)X]ClO_4 complexes, **4**–**6** ($X^- = Cl^-$, OH^-, or N_3^-) have distorted trigonal bipyramidal geometries in the solid state and have been characterized further by UV–vis absorption, electron paramagnetic resonance (EPR) spectroscopy, and cyclic voltammetry. The reaction of [Cu(**L2**)OH](ClO_4) (**5**) with H_2O_2 and *tert*-butyl hydroperoxide in methanol generates [Cu(**L2**)OOH](ClO_4) (**7**) and [Cu(**L2**)OO^{t}Bu](ClO_4) (**8**) which have been characterized by different spectroscopic methods. The compound [Cu(**L2**)OO^{t}Bu]$^+$ displays a band at 395 nm ($\epsilon = 950$ M^{-1} cm^{-1}) assigned to an alkylperoxo $\pi^*_\sigma \rightarrow$ Cu ligand-to-metal charge transfer (LMCT) transition, while [Cu(**L2**)OOH]$^+$ displays a peroxo $\pi^*_\sigma \rightarrow$ Cu charge-transfer transition at 365 nm with $\epsilon = 1300$ M^{-1} cm^{-1}, a mass ion at *m*/*z* 593.4, and ν_{O-O} stretch (resonance Raman) at 854 cm^{-1} that shifts to lower energy by 46 cm^{-1} upon ^{18}O substitution.

Introduction

Metal−hydroxo/(oxo) and metal−peroxo complexes are of interest because of their presence in many enzymatic reactions.[1,2] Of the three species, metal−peroxo complexes are generally more difficult to stabilize, and our understanding of their structures and properties has emerged through small molecule modeling studies. Both iron and copper proteins[1,3,4] are known to form peroxo (hydroperoxo) species involving one or two metals during important biological processes. Depending on the number of metal centers, copper enzymes can be divided into three general subfamilies.[4] The first group includes mononuclear species that require a cofactor to perform the reduction of dioxygen coupled to substrate oxidation (e.g., galactose and amine oxidase). The noncoupled binuclear copper proteins, peptidylglycine α-hydroxylating monooxygenase (PHM) and dopamine β-hydroxylase (Dβ H), constitute the second family, in which the metal centers are not magnetically coupled and are separated by more than 11 Å.[4] Oxygen reduction in these species appears to occur at only one copper center, and the resulting Cu/O_2 species are involved in subsequent reactions. Most likely, a side-on Cu(II)−superoxide is responsible for the C−H atom abstraction while the resulting Cu(II)−OOH species performs the eventual hydroxylation of the targeted substrate molecule.[5] The third subfamily contains trinuclear copper species as found in laccase and ascorbate oxidase.[6]

Small molecule modeling studies of copper metalloenzyme active sites have resulted in the preparation of many interesting and biologically relevant compounds.[7] Since the initial reports by Karlin and co-workers,[8a−f] subsequent

* To whom correspondence should be addressed. E-mail: bob.buchanan@louisville.edu. Phone: 502-852-6580. Fax: 502-852-8149.
[†] University of Louisville.
[‡] University of Cincinnati.

(1) Holm, R. H.; Kennepohl, P.; Solomon, E. I. *Chem. Rev.* **1996**, *96*, 2239−2314.
(2) MacBeth, C. E.; Gupta, R.; Mitchell-Koch, K. R.; Young, V. G.; Lushington, G. H.; Thompson, W. H.; Hendrich, M. P.; Borovik, A. S. *J. Am. Chem. Soc.* **2004**, *126*, 2556−2567.
(3) Que, L.; Tolman, W. B. *Angew. Chem., Int. Ed.* **2002**, *41*, 1114−1137.
(4) (a) Decker, A.; Solomon, E. I. *Curr. Opin. Chem. Biol.* **2005**, *9*, 152−163. (b) Solomon, E. I.; Sundaram, U. M.; Machonkin, T. E. *Chem. Rev.* **1996**, *96*, 2563−2605.
(5) Chen, P.; Solomon, E. I. *J. Am. Chem. Soc.* **2004**, *126*, 4991−5000.
(6) Cole, A. P.; Root, D. E.; Mukherjee, P.; Solomon, E. I.; Stack, T. D. P. *Science* **1996**, *273*, 1848−1850.

10.1021/ic051280s CCC: $33.50
Published on Web 03/17/2006

studies by Solomon and co-workers,[8g,h] and initial reports by Kitajima and co-workers,[8i] interest in copper-peroxide chemistry has continued to stimulate studies focused on expanding our understanding of the structure and properties of these biologically important species. Many studies have examined the structure and properties of copper/peroxide compounds having 1:1 and 2:1 stoichiometries.[7] The 2:1 copper/peroxide species have been examined more extensively because the Cu_2O_2 unit is thermodynamically favored and readily stabilized at low temperatures.[7] Mononuclear Cu(II)−OOH species on the other hand are not as common as 2:1 copper/peroxide species, but they are important intermediates in oxidation reactions catalyzed by dopamine β-hydroxylase (DβH) and peptidylglycine α-hydroxylating monooxygenase (PHM).[9,10] To date, several mononuclear Cu−OOH species have been synthesized and characterized in a limited number of ligand environments,[11−17] and the structures of only two of them have been determined by X-ray crystallography.[11,12] In related studies, Karlin[18] and Kitajima[19] and co-workers have reported the synthesis, characterization, and X-ray crystal structures of mononuclear acylperoxo−Cu(II) complexes. In addition, Karlin and co-workers[8a−f,20] as well as others[21] have reported the spectroscopic properties of several binuclear hydroperoxo−Cu(II) complexes.

The Cu atoms in many copper proteins are usually coordinated to two or more histidine residues associated with the primary coordination sphere. As in many enzymatic processes, neighboring active site amino acid residues appear to play an important role in binding and activating substrate molecules or cofactors via weak intermolecular forces, such as hydrogen-bonding, hydrophobic, hydrophilic, and electrostatic interactions. These neighboring amino acid residues are often referred to as "second coordination sphere" ligands,[22] and their importance in stabilizing reactive intermediates in enzymatic processes has stimulated the design of new biomimetic compounds for modeling studies.[23−26]

Several ligand designs have been developed to probe the effects of the second coordination sphere on metal coordination and endogenous ligand bonding and stabilization. Generally, these ligands are capable of forming intra- and intermolecular hydrogen bonds to coordinated endogenous ligands or outer-sphere exogenous molecules,[25a] and they possess sufficient steric bulk to prevent the formation of multimetallic species. The latter property is particularly important in stabilizing mononuclear compounds over dinuclear and aggregated species. Another desirable property associated with the design of such ligands is the ability to manipulate the structure and properties of the resulting polypodal

(7) (a) Solomon, E. I.; Chen, P.; Metz, M.; Lee, S. K.; Palmer, A. E. *Angew. Chem., Int. Ed.* **2001**, *40*, 4570−4590. (b) Mirica, L. M.; Ottenwaelder, X.; Stack, T. D. P. *Chem. Rev.* **2004**, *104*, 1013−1045. (c) Lewis, E. A.; Tolman, W. B. *Chem. Rev.* **2004**, *104*, 1047−1076. (d) Hatcher, L. Q.; Karlin, K. D. *J. Biol. Inorg. Chem.* **2004**, *9*, 669−683.

(8) (a) Liang, H. C.; Dahan, M.; Karlin, K. D. *Curr. Opin. Chem. Biol.* **1999**, *3*, 168−175. (b) Ghosh, P.; Tyeklar, Z.; Karlin, K. D.; Jacobson, R. R.; Zubieta, J. *J. Am. Chem. Soc.* **1987**, *109*, 6889−6891. (c) Jacobson, R. R.; Tyeklar, Z.; Farooq, A.; Karlin, K. D.; Liu, S.; Zubieta, J. *J. Am. Chem. Soc.* **1988**, *110*, 3690−3692. (d) Karlin, K. D.; Ghosh, P.; Cruse, R. W.; Farooq, A.; Gultneh, Y.; Jacobson, R. R.; Blackburn, N. J.; Strange, R. W.; Zubieta, J. *J. Am. Chem. Soc.* **1988**, *110*, 6769−6780. (e) Karlin, K. D.; Cruse, R. W.; Gultneh, Y. *Chem. Commun.* **1987**, 599−600. (f) Karlin, K. D.; Cruse, R. W.; Gultneh, Y.; Hayes, J. C.; Zubieta, J. *J. Am. Chem. Soc.* **1984**, *106*, 3372−3374. (g) Baldwin, M. J.; Ross, P. K.; Pate, J. E.; Tyeklar, Z.; Karlin, K. D.; Solomon, E. I. *J. Am. Chem. Soc.* **1991**, *113*, 8671−8679. (h) Pate, J. E.; Cruse, R. W.; Karlin, K. D.; Solomon, E. I. *J. Am. Chem. Soc.* **1987**, *109*, 2624−2630. (i) Kitajima, N.; Fujisawa, K.; Fujimoto, C.; Morooka, Y.; Hashimoto, S.; Kitagawa, T.; Toriumi, K.; Tatsumi, K.; Nakamura, A. *J. Am. Chem. Soc.* **1992**, *114*, 1277−1291.

(9) (a) Chen, P.; Solomon, E. I. *Proc. Natl Acad. Sci. U.S.A.* **2004**, *101*, 13105−13110. (b) Chen, P.; Bell, J.; Eipper, B. A.; Solomon, E. I. *Biochemistry* **2004**, *43*, 5735−5747.

(10) (a) Evans, J. P.; Ahn, K.; Klinman, J. P. *J. Biol. Chem.* **2003**, *278*, 49691−49698. (b) Francisco, W. A.; Blackburn, N. J.; Klinman, J. P. *Biochemistry* **2003**, *42*, 1813−1819. (c) Kamachi, T.; Kihara, N.; Shiota, Y.; Yoshizawa, K. *Inorg. Chem.* **2005**, *44*, 4226−4236.

(11) Chen, P.; Fujisawa, K.; Solomon, E. I. *J. Am. Chem. Soc.* **2000**, *122*, 10177−10193.

(12) Wada, A.; Harata, M.; Hasegawa, K.; Jitsukawa, K.; Masuda, H.; Mukai, M.; Kitagawa, T.; Einaga, H. *Angew. Chem., Int. Ed.* **1998**, *37*, 798−799.

(13) (a) Yamaguchi, S.; Nagatomo, S.; Kitagawa, T.; Funahashi, Y.; Ozawa, T.; Jitsukawa, K.; Masuda, H. *Inorg. Chem.* **2003**, *42*, 6968−6970. (b) Yamaguchi, S.; Kumagai, A.; Nagatomo, S.; Kitagawa, T.; Funahashi, Y.; Ozawa, T.; Jitsukawa, K.; Masuda, H. *Bull. Chem. Soc. Jpn.* **2005**, *78*, 116−124. (c) Yamaguchi, S.; Wada, A.; Nagatomo, S.; Kitagawa, T.; Jitsukawa, K.; Masuda, H. *Chem. Lett.* **2004**, *33*, 1556−1557. (d) Fujii, T.; Naito, A.; Yamaguchi, S.; Wada, A.; Funahashi, Y.; Jitsukawa, K.; Nagatomo, S.; Kitagawa, T.; Masuda, H. *Chem. Commun.* **2003**, 2700−2701.

(14) Ohta, T.; Tachiyama, T.; Yoshizawa, K.; Yamabe, T.; Uchida, T.; Kitagawa, T. *Inorg. Chem.* **2000**, *39*, 4358−4369.

(15) Ohtsu, H.; Itoh, S.; Nagatomo, S.; Kitagawa, T.; Ogo, S.; Watanabe, Y.; Fukuzumi, F. *Inorg. Chem.* **2001**, *40*, 3200−3207.

(16) Osako, T.; Nagatomo, S.; Tachi, Y.; Kitagawa, T.; Itoh, S. *Angew. Chem., Int. Ed.* **2002**, *41*, 4325−4328.

(17) Kodera, M.; Kita, T.; Miura, I.; Nakayama, N.; Kawata, T.; Kano, K.; Hirota, S. *J. Am. Chem. Soc.* **2001**, *123*, 7715−7716.

(18) (a) Sanyal, I.; Ghosh, P.; Karlin, K. D. *Inorg. Chem.* **1995**, *34*, 3050−3056. (b) Ghosh, P.; Tyeklar, Z.; Karlin, K. D.; Jacobson, R. R.; Zubieta, J. *J. Am. Chem. Soc.* **1987**, *109*, 6889−6891.

(19) Kitajima, N.; Fujisawa, K.; Morooka, Y. *Inorg. Chem.* **1990**, *29*, 357−358.

(20) (a) Murthy, N. N.; Mahroof-Tahir, M.; Karlin, K. D. *Inorg. Chem.* **2001**, *40*, 628−635. (b) Root, D. E.; Mahroof-Tahir, M.; Karlin, K. D.; Solomon, E. I. *Inorg. Chem.* **1998**, *37*, 4838−4848. (c) Mahroof-tahir, M.; Murthy, N. N.; Karlin, K. D.; Blackburn, N. J.; Shaikh, S. N.; Zubieta, J. *Inorg. Chem.* **1992**, *31*, 3001−3003.

(21) (a) Itoh, K.; Hayashi, H.; Furutachi, H.; Matsumoto, T.; Nagatomo, S.; Tosha, T.; Terada, S.; Fujinami, S.; Suzuki, M.; Kitagawa, T. *J. Am. Chem. Soc.* **2005**, *127*, 5212−5223. (b) Teramae, S.; Osako, T.; Nagatomo, S.; Kitagawa, T.; Fukuzumi, S.; Itoh, S. *J. Inorg. Biochem.* **2004**, *98*, 746−757.

(22) Karlin, S.; Zhu, Z. Y.; Karlin, K. D. *Proc. Natl. Acad. Sci. U.S.A.* **1997**, *94*, 14225−14230.

(23) (a) Harata, M.; Hasegawa, K.; Jitsukawa, K.; Masuda, H.; Einaga, H. *Bull. Chem. Soc. Jpn.* **1998**, *71*, 1031−1038. (b) Harata, M.; Jitsukawa, K.; Masuda, H.; Einaga, H. *Bull. Chem. Soc. Jpn.* **1998**, *71*, 637−645. (c) Wada, A.; Honda, Y.; Yamaguchi, S.; Nagatomo, S.; Kitagawa, T.; Jitsukawa, K.; Masuda, H. *Inorg. Chem.* **2004**, *43*, 5725−5735. (d) Jitsukawa, K.; Harata, M.; Arii, H.; Sakurai, H.; Masuda, H. *Inorg. Chim. Acta* **2001**, *324*, 108−116.

(24) (a) Tubbs, K. J.; Fuller, A. L.; Bennett, B.; Arif, A. M.; Berreau, L. M. *Inorg. Chem.* **2003**, *42*, 4790−4791. (b) Tubbs, K. J.; Fuller, A. L.; Bennett, B.; Arif, A. M.; Makowska-Grzyska, M. M.; Berreau, L. M. *J. Chem. Soc., Dalton Trans.* **2003**, 3111−3116.

(25) (a) Borovik, A. S. *Acc. Chem. Res.* **2005**, *38*, 54−61. (b) Gupta, R.; Borovik, A. S. *J. Am. Chem. Soc.* **2003**, *125*, 13234−13242. (c) MacBeth, C. E.; Hammes, B. S.; Young, V. G.; Borovik, A. S. *Inorg. Chem.* **2001**, *40*, 4733−4741.

(26) (a) Shirin, Z.; Carrano, C. J. *Polyhedron* **2004**, *23*, 239−244. (b) Hammes, B. S.; Luo, X.; Carrano, M. W.; Carrano, C. J. *Angew. Chem., Int. Ed.* **2002**, *41*, 3259−3262. (c) Hammes, B. S.; Luo, X. M.; Chohan, B. S.; Carrano, M. W.; Carrano, C. J. *J. Chem. Soc., Dalton Trans.* **2002**, 3374−3380. (d) Hammes, B. S.; Carrano, M. W.; Carrano, C. J. *J. Chem. Soc., Dalton Trans.* **2001**, 1448−1451.

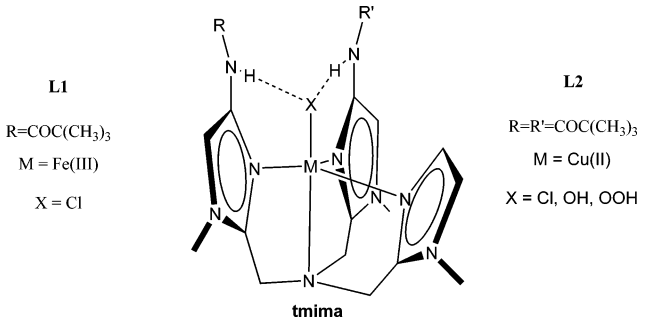

Figure 1. Illustration of the amide functionalized polyimidazole metal binding pocket.

frameworks to probe the effect of hydrophobicity and hydrophilicity on second coordination sphere interactions.

Many recent studies examining second coordination sphere effects have focused on the synthesis of ligands capable of stabilizing mononuclear M−O(H) and M−OOH species as models of unstable and reactive intermediates in enzymatic processes. Masuda and co-workers[13,23] and Berreau and co-workers[24] have used tripodal pyridine ligands containing amide pendants to stabilize hydroxide and hydroperoxide species bound to Fe and Cu. Borovik and co-workers[25] have utilized urea-based amine tripods to stabilize metal−hydroxo and high valence metal−oxo species. More recently, Carrano and co-workers[26] have explored second coordination sphere effects with the use of carboxamide and 3-carboxyethyl functionalized pyrazolate ligands. These ligand systems exploit the hydrogen-bonding properties of amide, urea, carboxamide, and 3-carboxyethyl functionalities to examine second coordination sphere interactions in respective metal complexes.

Our lab has evaluated the use of tris((1-methyl-imidazol-2-yl)methyl)amine (tmima)[27] as a model of histidine residues found in the primary coordination sphere of many metalloenzymes.[28] As with other N_4 tripodal ligands, tmima readily forms coordination complexes with different metals,[27] and the synthetic procedures used to prepare tmima are easily modified to prepare other derivatives, making tmima a useful scaffold for the construction of polypodal ligand frameworks to probe second coordination sphere interactions. In addition, another important feature of tmima and its derivatives is that they contain biological relevant imidazole donors that more closely mimic the imidazole group of histidine.

For example, recently we reported the structure and properties of an Fe(III) complex containing a new amide functionalized imidazole tripod, **L1**, shown in Figure 1.[29] The polyimidazole ligand contains an amide pendant in the fourth position of the imidazole ring that is properly positioned to form intramolecular six-membered hydrogen-bonding rings with ligands bonded cis to the functionalized imidazole donor. The present study describes our efforts to expand the use of tmima as a biomimetic imidazole scaffold and describes the synthesis and properties of a new amide functionalized imidazole tripod, **L2**, which contains two amide pendants. This ligand illustrates further the potential use of properly positioned amide pendants in stabilizing reactive and unstable species such as M−OH and M−OOH, mimicking the effects of the second coordination sphere in enzymatic processes.

Complexes included in this study have been characterized by several physical methods including X-ray crystallography, ESI-MS spectrometry, UV−vis absorption, electron paramagnetic resonance (EPR), and resonance Raman spectroscopy, and the results from these studies are compared with those reported for related systems.

Experimental Section

Materials and Methods. All chemicals obtained from commercial sources were reagent grade and used as received. 2-Aminomethyl-1-methylimidazole was prepared according to a previously published procedure.[27d] Deuterated solvents were obtained from Cambridge Isotope Laboratories.

Physical Methods. Infrared spectra were recorded on a Mattson Galaxy series 5000 FTIR using the diffuse reflectance infrared Fourier transform spectra (DRIFTS) mode. The spectra were recorded on samples prepared with dried KBr matrix. A SPEX 1404 0.85 m double spectrometer equipped with a liquid N_2 cooled 13.6 mm back-thinned SPEX Spectrum-1 CCD chip detector was used to collect Raman spectra. Raman scattering was excited by the 488.0 nm line of a Coherent 10 W Sabre Ar ion laser. A 200 mW power was used to excite samples because they were found to photodecompose at higher power settings. The scattered light was directed through a Kaiser Optical Systems Holographic SuperNotch filter. Raman shifts were calibrated against the appropriate Raleigh scattering line. A methanol solution of the sample to be analyzed was cooled prior to the data acquisition in a capillary tube to approximately −100 °C by a liquid N_2 stream blown through a quartz EPR-type cooling tube (Bruker Instruments). Baselines of resulting spectra were corrected using a four-point correction method using GRAMS/32 (version 5.22). Multiple spectra were averaged to improve the signal-to-noise ratios. Electronic spectra between 300 and 800 nm were recorded on a Cary 50 biospectrophotometer using 1 cm path length cells. Low-temperature absorption spectra of **6** and **7** were recorded in CH_3OH at −40 °C. X-band (9.03 GHz) EPR spectra were recorded on a Varian Associates E-109 spectrometer. The magnetic field was calibrated using a Varian E-500 NMR gauss meter. An insert Dewar filled with liquid nitrogen (77 K) was used for low-temperature measurements. EPR spectra were simulated using the WINEPR SimFONIA program version 1.25. ^{1}H and ^{13}C NMR spectra were recorded on a three-channel Bruker UnityInova 500 MHz spectrometer complete with pulse-field gradient capability. Voltammetric measurements were conducted using a PAR 173 potentiostat, a PAR 175 universal programmer, a PAR digital coulometer, and a Houston Instruments 2000 *X*−*Y* plot recorder. Electrochemical experiments were performed in dry acetonitrile containing tetrabutylammonium perchlorate (0.1 M) as the supporting electrolyte under an inert nitrogen atmosphere. A standard three-electrode cell, consisting of a glassy-carbon working electrode, Ag/AgCl reference electrode, and a

(27) (a) Chen, S.; Richardson, J. F.; Buchanan, R. M. *Inorg. Chem.* **1994**, *33*, 2376−2382. (b) Oberhausen, K. J.; Obrien, R. J.; Richardson, J. F.; Buchanan, R. M. *Inorg. Chim. Acta* **1990**, *173*, 145−154. (c) Oberhausen, K. J.; Obrien, R. J.; Richardson, J. F.; Buchanan, R. M.; Costa, R.; Latour, J. M.; Tsai, H. L.; Hendrickson, D. N. *Inorg. Chem.* **1993**, *32*, 4561−4565. (d) Oberhausen, K. J.; Richardson, J. F.; Buchanan, R. M.; Pierce, W. *Polyhedron* **1989**, *8*, 659−668.
(28) Varfolomeev, S. D.; Gurevich, K. G. *Russ. Chem. Bull.* **2001**, *50*, 1709−1717.
(29) Cheruzel, L. E.; Wang, J. P.; Mashuta, M. S.; Buchanan, R. M. *Chem. Commun.* **2002**, 2166−2167.

Table 1. Summary of Crystallographic Data for **L2** and **4**−**6**

	L2·H_2O·C_6H_{14}[a] $C_{25}H_{39}N_9O_2$·H_2O·C_6H_{14}	**4**·$2C_4H_{10}O$[a] [Cu(**L2**)Cl]$^+$·ClO_4·$2C_4H_{10}O$	**5**·$C_4H_{10}O$[a] 2([Cu(**L2**)OH]$^+$·ClO_4)·$C_4H_{10}O$	**6** [Cu(**L2**)N_3]$^+$·ClO_4
formula	$C_{31}H_{55}N_9O_3$	$C_{33}H_{59}CuN_9O_8Cl_2$	$C_{54}H_{90}CuN_9O_8Cl$	$C_{25}H_{39}CuN_{12}O_6Cl$
fw	601.85	844.34	1429.44	702.67
cryst syst	monoclinic	monoclinic	monoclinic	triclinic
space group	*C*2/*c*	$P2_1/c$	$P2_1/n$	$P\bar{1}$
a, Å	29.757(6)	18.908(9)	21.653(10)	12.003(3)
b, Å	11.358(2)	20.140(9)	10.260(5)	12.133(3)
c, Å	19.493(4)	11.196(5)	31.194(15)	13.327(3)
α, deg				116.114(4)
β, deg	97.948(3)	94.606(8)	93.766(8)	103.539(4)
γ, deg				99.520(4)
V, Å^3	6525(2)	4250(3)	6915(6)	1612.2(7)
Z	8	4	4	2
D_{calcd}, g/cm^3	1.225	1.318	1.372	1.447
cryst size, mm^3	0.45 × 0.25 × 0.15	0.37 × 0.25 × 0.12	0.32 × 0.25 × 0.11	0.17 × 0.08 × 0.04
μ(Mo Kα), cm^{-1}	0.072	0.680	0.760	0.819
F(000)	2224	1452	2818	734
temp, K	100(2)	100(2)	100(2)	293(2)
2*θ* range, deg	3.84−56.08	5.44−50.46	3.78−50.36	3.62−50.24
reflns collected	27922	29070	49657	12004
unique reflns	7543	7445	12328	5712
R_{int}	0.023	0.111	0.115	0.079
no. of observations	7543 ($I > 2\sigma(I)$)	7445 ($I > 2\sigma(I)$)	12328 ($I > 2\sigma(I)$)	5712 ($I > 2\sigma(I)$)
no. of variables	359	359	758	417
refln/param ratio	21.01	20.74	16.26	13.70
R1[b]	0.068	0.074	0.086	0.065
wR2[c]	0.126	0.138	0.165	0.113
GOF	1.03	1.06	1.05	1.01
max/min peak, e/Å^3	0.59/−0.39	0.56/−0.59	0.60/−0.62	0.51/−0.46

[a] Solvate molecules are not included in formula and formula weight and were removed using the SQUEEZE program. [b] $R1 = \sum||F_o| - |F_c||/\sum|F_o|$. [c] $wR2 = \{\sum[w(F_o^2 - F_c^2)^2]/\sum[w(F_o^2)^2]\}^{1/2}$, where $w = q/\sigma^2(F_o^2) + (qp)^2 + bp$. GOF $= S = \{\sum[w(F_o^2 - F_c^2)^2]/(n - p)\}^{1/2}$.

platinum coil auxiliary electrode, was used to conduct electrochemical measurements. The ferrocenium/ferrocene couple was measured under the same conditions to correct for the junction potentials as both an internal and external reference. All redox potentials are reported relative to the ferrocenium/ferrocene couple of 0.44 mV versus Ag/AgCl.

X-ray Data Collection and Structural Determination. The crystal structures of compounds **L2** and **4**−**6** were determined as follows: A single crystal mounted on a glass fiber was used for collection of X-ray data on a Bruker SMART APEX CCD diffractometer. The SMART[30a] software package (version 5.628) was used to acquire 30 s *ω*-scan exposures of data at 100(2) K using monochromatic Mo Kα radiation (0.71073 Å) from a sealed tube and a monocapillary. Frame data were processed using SAINT[30b] (version 6.36) to determine final cell parameters (see Table 1) and to generate raw *hkl* data that were then corrected for absorption using SADABS[30c] (version 2.02). The structures were solved by direct methods (**L2** and **5**) and Patterson methods (**4** and **6**) using SHELXS-90[30d] and refined by least-squares methods on F^2 using SHELXL-99[30e] incorporated into the SHELXTL 6.12[30f] suite of programs. All non-hydrogen atoms of the cations were refined anisotropically except for **4**. Hydrogen atoms, perchlorate couterions, and *tert*-butyl groups were modeled adequately for each structure, and the contribution from the solvent molecules were removed using SQUEEZE[31] (see Supporting Information). Additional details for the compounds including atomic coordinates and anisotropic displacement parameters, as well as complete lists of bond lengths, angles, and torsion angles, are available in CIF format in Supporting Information.

Preparation of L2 and Metal Complexes. *N,N*-Bis((1-methyl-4-nitroimidazol-2-yl)methyl)-*N′*-((1-methylimidazol-2-yl)-methyl)amine (1). A solution (25 mL) containing 0.16 g (1.03 mmol) of 1-methyl-4-nitroimidazole-2-carboxaldehyde[32] and 0.05 g (0.47 mmol) of 2-aminomethyl-1-methylimidazole[27d] in anhydrous methanol was reacted with 0.14 g (2.22 mmol) of $NaBH_3CN$ in the presence of 200 μL of glacial acetic acid. After 2 h, the reaction mixture was quenched with 3 M hydrochloric acid, and after the appropriate workup,[27a] **1** was isolated as a pale yellow oil (60% yield). ***Caution:*** *Cyanide is extremely toxic, and appropriate safety precautions should be followed at the initial stage of the workup procedure.* IR (film): 1657 and 1456 cm^{-1} (NO_2). ^{1}H NMR $CDCl_3$ *δ* 7.59 (s, 2, ^{NO2}Im(H-5)), 6.96 (s, 1, H-5), 6.80 (s, 1, H-4), 4.04 (s, 2, CH_2), 4.05 (s, 4, ^{NO2}Im(CH_2)), 3.77 (s, 3, CH_3), 3.76 (s, 6, ^{NO2}Im(CH_3)); ^{13}C NMR $CDCl_3$ *δ* 146.9 (s, ^{NO2}C-2), 146.2 (s, ^{NO2}C-4), 130.7 (s, C-2), 127.1 (s, C-4), 121.9 (s, ^{NO2}C-5), 121.7 (s, ^{NO2}C-5), 56.9 (s, $^{NO2}CH_2$, CH_2), 34.3 (s, $^{NO2}CH_3$), 33.2 (s, CH_3). HRMS for $C_{15}H_{19}N_9O_4$: calcd, 390.1638 (M + H^+); found, 390.1669. Anal. Calcd for $C_{15}H_{19}N_9O_4$: C, 46.26; H, 4.92; N, 32.38. Found: C, 46.80; H, 4.86; N, 32.52.

***N,N*-Bis((1-methyl-4-pivalamidoimidazol-2-yl)methyl)-*N′*-((1-methylimidazol-2-yl)methyl)amine (L2).** The pale yellow oil of **1** (0.13 g (0.33 mmol)) in 25 mL of anhydrous methanol was reduced in the presence of 0.12 g of 5% Pd/C and 0.94 mL (1.65

(30) (a) *SMART*, version 5.625; Bruker Advanced X-ray Solutions, Inc.: Madison, WI, 2001. (b) *SAINT*, version 6.22; Bruker Advanced X-ray Solutions, Inc.: Madison, WI, 2001. (c) Sheldrick, G. M. *SADABS: Area Detector Absorption Correction*, version 2.02; University of Göttingen: Göttingen, Germany, 1997. (d) Sheldrick, G. M. SHELXS-90. *Acta Crystallogr*. **1990**, *A46*, 467. (e) Sheldrick, G. M. *SHELXL-99: Program for the Refinement of Crystal Structures;* University of Göttingen: Göttingen, Germany, 1997. (f) *SHELXTL, Program Library for Structure Solution and Molecular Graphics*, version 6.12; Bruker Advanced X-ray Solutions: Madison, WI, 2001.

(31) Spek, A. L. *SQUEEZE;* University of Utrecht: Utrecht, The Netherlands, 1992. SQUEEZE is a routine implemented in PLATON-92 allowing solvent contributions to be eliminated from the reflection data.

(32) Cheruzel, L. E.; Mashuta, M. S.; Buchanan, R. M. *Chem. Commun.* **2005**, 2223−2225.

Scheme 1. Illustration of the Reaction Scheme Followed during the Synthesis of **1** and **L2**

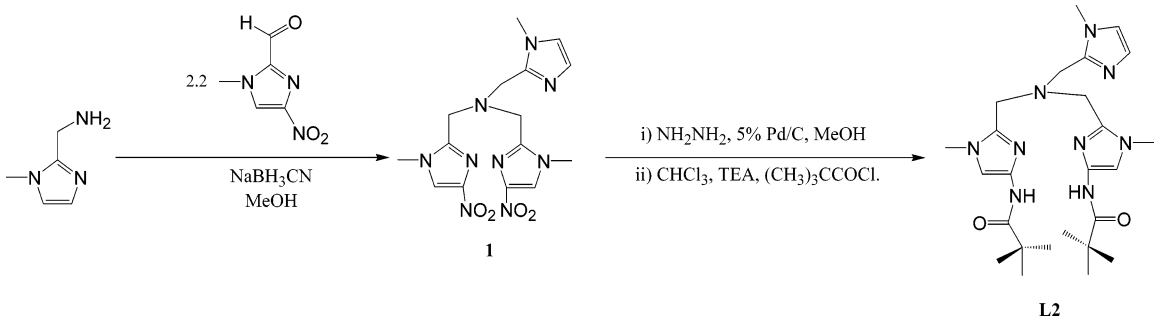

mmol) of hydrazine monohydrate.[33] After 4 h, the catalyst was carefully filtered through Celite, and the methanol filtrate was poured into 50 mL of water. After evaporation of the methanol, the aqueous solution was extracted four times with 15 mL of chloroform, and the organic layer was dried over magnesium sulfate. Triethylamine (119 μL (0.86 mmol)) and 96 μL (0.79 mmol) of pivaloyl chloride were added slowly and sequentially to the dry dichloromethane solution. After 2 h, removal of the solvent yielded 72 mg (43%) of crude **L2** as a yellow oil, which was then purified by column chromatography (silica gel, solvent CH_2Cl_2 and gradient of MeOH (2:1) ratio, $R_f = 0.4$). IR (KBr): 3052 cm^{-1} (amide−NH), 1667 cm^{-1} (amide−C═O). ^{1}H NMR CD_2Cl_2 δ 7.81 (s, ^{Am}Im(N−H)), 7.09 (s, 2, ^{Am}Im(H-5)), 6.80 (s, 1, Im(H-5)), 6.75 (s, 1, Im(H-4)), 3.60 (s, 2, Im(−CH_2)), 3.57 (s, 4, ^{Am}Im(CH_2)), 3.07 (s, 3, Im(−CH_3)), 3.02 (s, 6, ^{Am}Im(−CH_3)), 1.18 (s, 18, ^{Am}Im(−C(CH_3)$_3$)); ^{13}C NMR $CDCl_3$ δ 174.1, (s, ^{Am}Im(−C═O)), 145.4 (s, Im(C-2)), 141.2 (s, ^{Am}Im(C-4)), 135.5 (s, ^{Am}Im(C-2)), 126.4 (s, Im(C-4)), 120.8 (s, Im(C-5)), 107.9 (s, ^{Am}Im(C-5)), 47.8 (s, Im(−CH_2−), ^{Am}Im(−CH_2−)), 38.0 (s, ^{Am}Im(N−$\underline{C}H_3$)), 31.1 (s, Im(CH_3)), 28.9 (s, ^{Am}Im($\underline{C}(CH_3)_3$, ^{Am}Im(C($\underline{C}H_3)_3$). HRMS for $C_{25}H_{30}N_9O_2$: calcd, 498.3305 (M + H$^+$); found, 498.3311.

Preparation of Metal Complexes. [Cu(L2)](ClO$_4$)$_2$ (2). To **L2** (0.24 g (0.47 mmol)) dissolved in 2 mL of methanol was added dropwise a 1 mL methanol solution containing 0.17 g (0.47 mmol) of copper(II) perchlorate hexahydrate. The green solution was then layered with 10 mL of ether and stored at −20 °C, and the resulting green precipitate of [Cu(**L2**)](ClO$_4$)$_2$ (**2**) formed overnight (75% yield). The ESI-MS spectrum of **2** showed two positive ions with peak clusters at *m*/*z* 559.3 ([Cu(**L2**−H)]$^+$) and *m*/*z* 659.3 ([Cu(**L2**)]ClO$_4^+$). The UV−vis spectrum of **2** in methanol displayed two transitions at 415 nm (ϵ = 100 M^{-1} cm^{-1}) and 725 nm (ϵ = 70 M^{-1} cm^{-1}). Compound **2** displays a quasi-reversible one-electron redox couple in acetonitrile at $E_{1/2}$ = −150 mV (versus Ag/AgCl).

[Cu(tmima)](ClO$_4$)$_2$ (3). Compound **3** was synthesized following the same general procedure outlined for **2**. Briefly, a 1 mL methanol solution of tmima (0.10 g (0.33 mmol)) was treated with a 1 mL methanol solution containing 0.12 g (0.33 mmol) of copper(II) perchlorate hexahydrate. After the green solution was layered with ether (10 mL), a green precipitate formed and was collected through vacuum filtration giving 98 mg of **3** (52%). The ESI-MS spectrum of **3** showed two positive ions with peak clusters at *m*/*z* 362.2 ([Cu(tmima)]$^+$) and *m*/*z* 461.1 ([Cu(tmima)]ClO$_4^+$). The UV−vis spectrum of **3** in methanol displayed one d−d transition at 635 nm (ϵ = 80 M^{-1} cm^{-1}). Compound **3** displays a quasi-reversible one-electron redox couple in acetonitrile at $E_{1/2}$ = −110 mV (versus Ag/AgCl).

[Cu(L2)Cl](ClO$_4$) (4). The [Cu(**L2**)Cl]$^+$ complex was prepared by adding 100 μL of saturated NaCl to a 8 mM stock methanol solution (2 mL) of [Cu(**L2**)](ClO$_4$)$_2$. The green methanolic solution (transitions at 795 nm (ϵ = 50 M^{-1} cm^{-1}) was then layered with ether and stored at −20 °C. Large brown X-ray quality crystals (4.5 mg) of **4** formed overnight (48% yield). ESI-MS: *m*/*z* 596.4 [Cu(**L2**)Cl]$^+$. $E_{1/2}$ = −160 mV (in acetonitrile versus Ag/AgCl).

[Cu(L2)OH](ClO$_4$) (5). Compound **5** was prepared as follows: to the 8 mM stock methanolic solution (2 mL) of compound **2** was added 2.3 μL (0.03 mmol) of triethylamine. Slow evaporation of methanol/ether yielded green X-ray quality plates (58% yield). ESI-MS: *m*/*z* 577.2 [Cu(**L2**)OH]$^+$. UV−vis (MeOH): 315 nm (ϵ = 2380 M^{-1} cm^{-1}) and 725 nm (ϵ = 140 M^{-1} cm^{-1}).

[Cu(L2)N$_3$](ClO$_4$) (6). Compound **6** was prepared as follows: to the 8 mM stock methanolic solution (2 mL) of **2** was added 10 mg (0.2 mmol) of sodium azide in 0.5 mL of water. Layering the solution with ether produced dark green crystals (74% yield) suitable for X-ray analysis. The UV−vis spectrum of **6** in methanol displays two transitions at 385 nm (ϵ = 450 M^{-1} cm^{-1}) and 690 nm (ϵ = 50 M^{-1} cm^{-1}). Its electrochemical behavior in acetonitrile (0.1 M TBAP) is irreversible, differing from the reversible one-electron process observed for a series of related Cu(II)−azido complexes containing pyridine ligands.[13,23−24]

Reactions of [Cu(L2)]ClO$_4$ (2) with Hydrogen Peroxide and *tert*-Butyl Hydroperoxide. [Cu(**L2**)OOH](ClO$_4$) (**7**) and [Cu(**L2**)-OO^{t}Bu](ClO$_4$) (**8**) were prepared following the general procedure described above for **4**−**6**. The addition of 10 equiv of freshly prepared 30% H_2O_2 (0.01 mmol) to a 1 mM methanolic solution (1 mL) of compound **2** containing KOH (1 μmol) at −40 °C produces an immediate color change of the solution from green to yellow. The UV−vis spectrum of **7** displayed two transitions at 365 nm (ϵ = 1300 M^{-1} cm^{-1}) and 780 nm (ϵ = 240 M^{-1} cm^{-1}). Compound **8** was prepared in a similar manner. The addition of 80 equiv of freshly prepared ^{t}BuOOH (0.08 mmol) to a 1 mM methanolic solution (1 mL) of compound **2** containing KOH (1 μmol) at −40 °C produces a slight color change of the solution from green to yellow-green. The UV−vis spectrum of **8** displayed two transitions at 390 nm (ϵ = 950 M^{-1} cm^{-1}) and 715 nm (ϵ = 140 M^{-1} cm^{-1}).

Results and Discussion

Synthesis and Characterization. The synthesis of **1** and **L2** and its corresponding Cu(II) complexes **2**−**8** is described in detail above. The 2-aminomethyl-1-methyl-imidazole precursor used in the synthesis of **1** was prepared as described elsewhere[27d] and coupled with 1-methyl-4-nitro-imidazole-2-carboxaldehyde[32] in methanol in the presence of $NaBH_3CN$ and glacial acetic acid in ∼60% yield (see Scheme 1). The **L2** ligand was prepared by reduction of **1** in methanol in the presence of 5% Pd/C and hydrazine monohydrate.[33] The resulting diamine form of **1** is unstable

(33) Buchman, R.; Heinstei, P. F.; Wells, J. N. *J. Med. Chem.* **1974**, *17*, 1168−1173.

and was not isolated. Rather, the methanol solution was poured into water, and after removal of the methanol under vacuum, the aqueous layer was extracted four times with chloroform. The organic layer was dried over magnesium sulfate and reacted with a slight excess of pivaloyl chloride containing triethylamine. Removal of the solvent produced a yellow oil of **L2** that was purified by column chromatography and isolated in 43% yield.

Analysis of an IR spectrum of **L2** shows the ν_{N-H} and $\nu_{C=O}$ amide stretches occur at 3052 and 1667 cm^{-1}, respectively. As expected, both **1** and **L2** have slightly different ^1H and ^{13}C NMR spectra (Figures S1−S4 in Supporting Information). Proton signals associated with the nitrated imidazole rings of **1** appear further downfield compared to signals of the unsubstituted imidazole ring. The methyl and methylene resonances associated with the nitrated rings also are shifted further downfield because of the electron-withdrawing nitro groups. **L2** displays similar chemical shift differences associated with the two types of imidazole rings and aliphatic protons resulting from the electron-withdrawing properties of the amide groups. The ^{13}C spectra on **1** and **L2** are consistent with the proposed structures, and corresponding assignments of proton signals of both compounds are listed in the Experimental Section. Compounds **1** and **L2** have been characterized further by HRMS, and the spectra of both compounds show $[M + H]^+$ ions consistent with their expected masses.

Both **L1**[29] and **L2** (Figure 1) serve as neutral ligands upon coordination to metals and represent rare examples of amide functionalized polyimidazole chelates.[34−36] As with **L1**, **L2** has a tripodal shape that encapsulates metals in a sterically hindered N_4 chelate pocket, and it possesses amide pendants capable of forming thermodynamically stable intramolecular six-membered rings with donor atoms of ligands coordinated in cis positions. **L2** readily stabilizes Cu(II) complexes containing different anion ligands. In this study, Cu(II) complexes of the general formula $[Cu(\mathbf{L2})X]^+$, where X = Cl^-, OH^-, or N_3^-, were synthesized using a stock solution of $[Cu(\mathbf{L2})](ClO_4)_2$ (**2**). The addition of the appropriate quantity of anion to an aliquot of the stock solution produced **4**−**6** in reasonable yields. The electronic absorption spectra of **4**−**6** were recorded in methanol and are consistent with other structurally related Cu(II) complexes.[27d] Compound **3** exhibited a d−d band centered at 795 nm (ϵ = 50 M^{-1} cm^{-1}). For **4**, the d−d band is centered at 725 nm (ϵ = 140 M^{-1} cm^{-1}), and an $OH^- \rightarrow$ Cu(II) LMCT transition is observed at 315 nm (ϵ = 2380 M^{-1} cm^{-1}). The electronic absorption spectrum of the azido complex **5** displays a d−d band at 700 nm (ϵ = 50 M^{-1} cm^{-1}) and a $N_3^- \rightarrow$ Cu(II) LMCT transition at 385 nm (ϵ = 450 M^{-1} cm^{-1}), which is notably weaker than the same transition reported for $[Cu(bppa)N_3]^+$.[23] The $[Cu(\mathbf{L2})OOH(^tBu)]^+$ species, **7** and **8**, were prepared by the addition of H_2O_2 (and ^{t}BuOOH) to a methanol solution of compound **5** generated in situ at −40 °C. The spectral properties of these species are discussed in more detail below and compared to the reactivity of the $[Cu(tmima)](ClO_4)_2$ (**3**), which lacks amide pendants.

Table 2. Selected Bond Distances (Å) and Angles (deg) for Complexes **4**−**6**

atoms	**4**	**5**	**6**
Cu−X[a]	2.265(2)	1.923(5)/1.954(7)	2.169(4)
Cu−N1	2.111(5)	2.189(6)/2.166(6)	2.058(5)
Cu−N2	1.970(5)	1.991(6)/1.996(8)	1.936(5)
Cu−N4	2.088(5)	2.032(6)/2.018(7)	1.978(5)
Cu−N6	1.974(5)	1.985(6)/2.002(7)	1.984(5)
N1−Cu−N2	82.2(2)	80.1(2)/80.0(3)	80.83(19)
N1−Cu−N4	80.1(2)	79.6(3)/78.6(3)	81.52(19)
N1−Cu−N6	80.4(2)	80.7(2)/80.0(3)	81.39(19)
N1−Cu−X	178.0(2)	173.1(2)/175.6(3)	176.0(2)
N2−Cu−N4	107.6(2)	113.4(2)/110.9(3)	106.2(2)
N2−Cu−N6	130.9(2)	122.6(4)/114.3(3)	112.6(2)
N2−Cu−X	99.8(2)	96.0(2)/96.4(3)	95.6(2)
N4−Cu−N6	114.0(2)	115.4(2)/114.3(3)	134.1(2)
N4−Cu−X	98.9(2)	97.0(2)/99.2(3)	101.3(2)
N6−Cu−X	98.5(2)	106.2(0)/105.3(3)	98.4(2)
Hydrogen-Bonding Parameters			
average N(amide)···X separation	3.293	2.875/3.056	3.094
average N(amide)−H···X angle	150.4	153.0/147.8	158.3

[a] X = Cl1 for **4**, O3 for **5**, and N10 for **6**.

X-ray Crystallography. The structures of complexes **L2** and compounds **4**−**6** have been determined by single-crystal X-ray methods. Details of the data collection and refinement are provided in Table 1 and are summarized below. Selected bond distances and angles are listed in Table 2. Illustrations showing closest intermolecular contacts between neighboring molecules in the crystal structures of **L2** and **4**−**6** are in Supporting Information.

Compound **L2** crystallizes as colorless blocks in the space group *C*2/*c* from ethyl acetate and hexane. The asymmetric unit contains one organic molecule and a water molecule, as well as a highly disordered hexane solvate. The distances and angles of the imidazole rings are normal and consistent with previously reported imidazole tripod compounds.[27,32] Interestingly, the **L2** molecule (Figure 2) adopts a similar paddle-wheel arrangement previously observed in the crystal structure of tmima[37] and its nitro-derivative.[32] The water molecule bridges two imidazole rings and is hydrogen-bonded to N4 and N6 (N4···O3 and N6···O3 separations of 2.858 and 2.781 Å, respectively, and O3−H3BO···N4 and O3−H3AO···N6 angles of 167.3° and 174.4°, respectively). In addition, one of the amide hydrogens, H8N, is strongly hydrogen-bonded to O3 with a N8···O3 separation of 2.830 Å and a N8−H8N···O3 angle of 152.7°. The remaining imidazole ring containing N2 is weakly hydrogen-bonded to the second amide hydrogen, H9N; the N2···N9 separation is 3.271 Å, and the N9−H9N···N2 angle is 157.5°. Two symmetry related imidazole rings containing N6 are involved in a slipped π-stack interaction[38] with the closest contact of 3.577 Å between C12 and C12′. The structure also contains

(34) Afreen, F.; Mathur, P.; Rheingold, A. *Inorg. Chim. Acta* **2005**, *358*, 1125−1134.
(35) Gupta, M.; Mathur, P.; Butcher, R. J. *Inorg. Chem.* **2001**, *40*, 878−885.
(36) Collman, J. P.; Zhong, M.; Costanzo, S.; Zhang, C. *J. Org. Chem.* **2001**, *66*, 8252−8256.
(37) Mashuta, M. S.; Cheruzel, L.; Buchanan, R. M. *Acta Crystallogr., Sect. C* **2002**, *58*, o629−o631.
(38) Janiak, C. *J. Chem. Soc., Dalton Trans.* **2000**, 3885−3896.

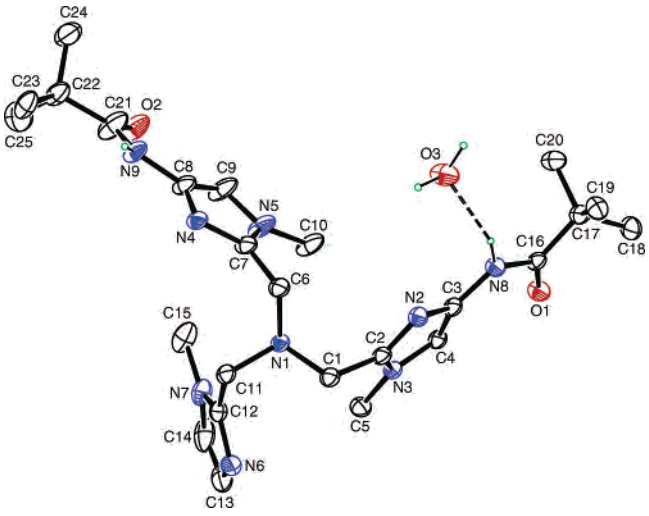

Figure 2. ORTEP view of the **L2** ligand hydrogen-bonded to a water molecule. Ellipsoids are drawn at 40% probability. Methyl, methylene, and imidazole hydrogens have been omitted for clarity.

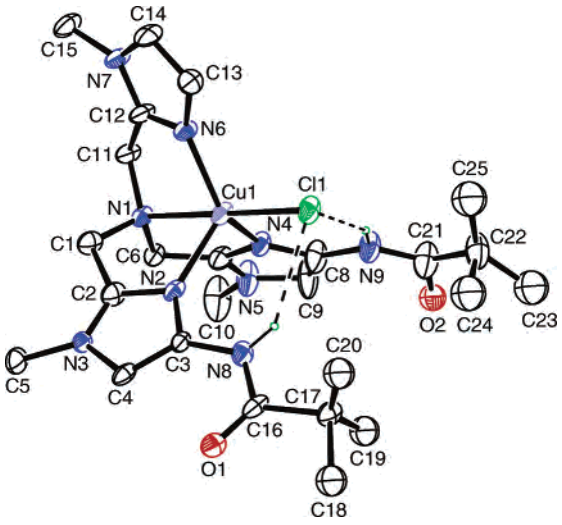

Figure 3. ORTEP view of the cation mononuclear copper complex of **4**. Ellipsoids are drawn at 40% probability level. Methyl, methylene, and imidazole hydrogens have been omitted for clarity.

weak intermolecular C−H···O interactions[39] between tripod molecules (Figure S5).

Crystal structures of the $[Cu(\mathbf{L2})X]^+$ complexes, with X = Cl^-, OH^-, and N_3^- (**4**−**6**), are shown respectively in Figures 3, 4 and 5 and discussed below. Selected distances and angles for each complex are presented in Table 2. Overall, the crystal structures of **4**−**6** reveal that the coordination geometries of the metal centers are best described as distorted trigonal bipyramidal with three imidazole nitrogen atoms occupying the equatorial plane and the tertiary amine nitrogen atom, N1, and the X anionic ligands occupying the apical positions. The Addison and Reedijk's τ parameter[40] for all three complexes are close to 1 (0.94, 0.85, and 0.70 for **4**, **5**, and **6**, respectively) and are nearly trigonal bipyramidal, with compound **6** having the most distorted coordination environment in the series. The

(39) Desiraju, G. R. *Acc. Chem. Res.* **1996**, *29*, 441−449.
(40) Addison, A. W.; Rao, T. N.; Reedijk, J.; Vanrijn, J.; Verschoor, G. C. *J. Chem. Soc., Dalton Trans.* **1984**, 1349−1356.

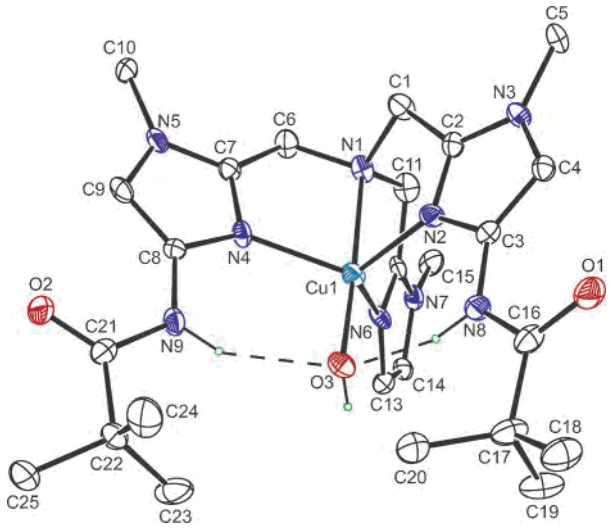

Figure 4. ORTEP view of the cation mononuclear copper complex of **5**. Ellipsoids are drawn at 40% probability level. Methyl, methylene, and imidazole hydrogens have been omitted for clarity.

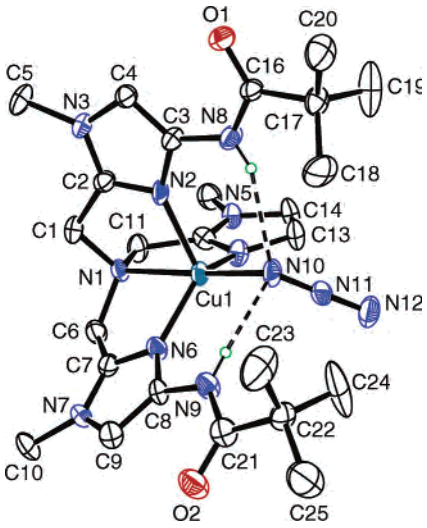

Figure 5. ORTEP view of the cation mononuclear copper complex of **6**. Ellipsoids are drawn at 40% probability level. Methyl, methylene, and imidazole hydrogens have been omitted for clarity.

bond distances and angles of the **L2** ligand in all three complexes are similar and consistent with those observed above for **L2**.

Compound **4** crystallizes in the monoclinic space group $P2_1/c$ with one Cu(II) cation and one perchlorate anion per asymmetric unit (Figure 3). The overall geometry of **4** resembles a slightly distorted trigonal bipyramid. Interestingly, a comparison of the bond distances and angles observed for **4**, and its previously reported parent compound $[Cu(tmima)Cl]^+$ (τ = 0.94), indicates that the **L2** ligand bonds more tightly to Cu(II) than tmima. Two of the Cu−N(Im) bonds in **4** are shorter by about 0.08 Å (Cu−N2 = 1.970(5) Å and Cu−N6 = 1.974(5) Å) as is the Cu−amine bond (Cu−N1 = 2.111(5) Å) by about 0.05 Å compared to $[Cu(tmima)Cl]^+$.[27] The shortening of the Cu−N1 distance in **4** results in an elongation of the Cu−Cl distance by 0.03 Å compared to $[Cu(tmima)Cl]^+$. The structural changes in **4** result in part from the increased steric

hindrance of the two *tert*-butyl groups on the **L2** ligand, as well as from the weak intramolecular interactions between the amide hydrogens and the axial chlorine atom (average Cl···N separation of 3.293 Å and N−H···Cl angle of 150.4°), which are within the range of hydrogen-bonding contacts established recently by Brammer et al.[41] The steric contact between the **L2** amide pendants in **4** also is reflected in the bond angles of the **L2** chelate donor atoms. While the bond angles associated with N1 in **4** are strikingly similar to the angles observed in $[Cu(tmima)Cl]^+$, the angles between N2, N4, and N6 in **4** reflect a greater distortion in its coordination environment. Unlike **L2**, the packing diagram of **4** only shows one weak intermolecular interaction in the solid state (Figure S6) involving a slipped face-to-face π-stack (3.438 Å) between neighboring imidazole ligands in the unit cell.

As previously mentioned, discreet mononuclear Cu(II)−OH complexes are usually difficult to isolate.[13d,24] Steric hindrance of **L2** has been exploited to prevent aggregation of the resulting Cu(II)−OH species, favoring isolation of a stable mononuclear complex instead. Compound **5** crystallizes in the monoclinic space group $P2_1/n$ with two independent Cu(II) complexes and perchlorate counterions per asymmetric unit (Figure 4). Both forms of **5** have distorted trigonal bipyrimidal geometries, near mirror symmetry, and very similar bond distances and angles (Table 2).

The Cu−N(Im) distances are normal and consistent with other reported Cu−N(Im) complexes[27] and, with the exception of the Cu−N1 distance, are similar to those observed in **4**. The average Cu−N(Im) distance in **5** is 0.1 Å shorter than the distances reported for related trigonal bipyramidal Cu−OH complexes containing pyridine−amide ligands, such as $[Cu(bppa)OH]^+$,[23] $[Cu(ebnpa)OH]^+$, and $[Cu(pbnpa)OH]^+$.[24] Interestingly, the average Cu−N(py) distance reported for the square planar $[Cu(bpba)MeOH]^{2+}$ complex, which contains a neutral coordinated methanol ligand, is 0.05 Å shorter than the Cu−N(Im) distances in **5**.[13d] The Cu−N1 distance (average 2.178(6) Å) in **5** is longer than in **4** and related to $[Cu(bppa)OH]^+$, $[Cu(ebnpa)OH]^+$, $[Cu(pbnpa)OH]^+$, and $[Cu(bpba)OH]^+$ complexes. Additionally, the average Cu−OH distance in **5** (1.924(5) Å) is longer than those reported for $[Cu(bppa)OH]^+$, $[Cu(ebnpa)OH]^+$, and $[Cu(pbnpa)OH]^+$ (average 1.880(2) Å) but shorter than the average value of 2.071 Å reported for $[Cu(bpba)MeOH]^{2+}$. The average N1−Cu−O3 angle in **5** is 174.4(2)° compared to 177.0(4)° (average) reported for the related trigonal bipyramidal pyridine−amide complexes above.

The two amide groups in **5** interact strongly with the hydroxyl oxygen atom, O3, and the average N···O separation is 2.875 Å with an N−H···O angle of 153.0°. The average N···O separation and N−H···O angle for the pyridine complexes above are 2.721 Å and 160.0°, respectively. The hydroxyl hydrogen atom is weakly hydrogen-bonded to the carbonyl oxygen of an amide pendant associated with the second molecule in the asymmetric unit (O3···O5 separation of 3.186 Å and O3−H3O···O5 angle of 158.24°) (Figure S7). Both of the amide hydrogen bonds appear to contribute to the longer than expected Cu−OH bond in **5** compared to the structurally related pyridine complexes. The packing diagram of **5** reveals edge-to-face (3.442 Å) and face-to-face (3.466 Å) π-stacks between neighboring imidazole rings of the independent Cu complexes (Figure S8).

Compound **6** crystallizes in the triclinic space group $P\bar{1}$ with one cationic Cu(II) complex and one perchlorate counterion per asymmetric unit (Figure 5). The distances and angles of the Cu and **L2** ligand are normal and similar to those observed in the structures of **L2**, **4**, and **5**. As with **4** and **5**, the coordination geometry of **6** is distorted trigonal bipyramidal and possesses near mirror symmetry. The axial azide ligand is bent with a Cu−N10−N11 angle of 119.5(3)° and has N−N distances consistent with other azido−Cu(II) complexes.[42]

The Cu−N1 distance (2.058(5) Å) is longer in **6** than in the related pyridine complexes, $[Cu(bppa)N_3]^+$ (1.987(7) Å),[23] $[Cu(ebnpa)N_3]^+$ (2.0214(18) Å),[24] and $[Cu(bpga)N_3]^+$ (1.999(5) Å).[13b] Also, the axial Cu−N(azide) distance (Cu−N10 = 2.169(4) Å) is longer than in the related pyridine complexes ($[Cu(bppa)N_3]^+$ (1.937(7) Å), $[Cu(ebnpa)N_3]^+$ (1.9652(19) Å), and $[Cu(bpga)N_3]^+$ (1.945(5) Å)). The two amide hydrogens are oriented toward N10 (azido) and have an average N···N10 distance of 3.094 Å and N−H···N10 angle of 158.3°. The two azide N−N bonds are different (N10−N11 distance of 1.210 and 1.144 Å for N11−N12) but typical of other Cu(II)−N_3 complexes.[42] As in compounds **4** and **5**, the average N···X separation and N−H···X angle indicate the hydrogen-bonding interaction of the **L2** amide pendants is slightly weaker than in structurally related pyridine complexes. This may be a result of the shorter Cu−N distances and more constrained chelate angles of the imidazole donor of **L2** compared to the related pyridine compounds. Weak intermolecular interactions such as π-stacking and C−H···N/O interactions are observed in **6** (Figures S9 and S10), which may be responsible for the greater distortion of its coordination environment compared to **4** and **5**, which have more regular trigonal bipyramidal geometries. The structure of **6** is relevant to the proposed Cu−OOH species (**7**) described below. End-on coordination of azide ligands has been used as a structural model of the coordination of the hydroperoxide ion in other studies.[43]

Overall, the crystal structures of **4**−**6** confirm that the **L2** ligand is capable of forming intramolecular hydrogen bonds with various axially coordinated anionic ligands, and the structures of these compounds are similar to the structures of related amide functionalized pyridine and amine−urea complexes.[23−26] The crystal structures of **4**−**6** indicate that the N···X separation decreases as X^- becomes a better hydrogen bond acceptor (e.g., $Cl^- < N^- < O^-$) suggesting the formation of stronger hydrogen bonds between amide hydrogen atoms and oxygen compared to that of nitrogen and chlorine.

(41) Brammer, L.; Bruton, E. A.; Sherwood, P. *Cryst. Growth Des.* **2001**, *1*, 277−290.

(42) Dori, Z.; Ziolo, R. F. *Chem. Rev.* **1973**, *73*, 247−254.

(43) Solomon, E. I.; Baldwin, M. J.; Lowery, M. D. *Chem. Rev.* **1992**, *92*, 521−542.

Table 3. EPR Parameters for the Cu(II) Complexes of **L2** in Frozen Methanol Solution

species	g	A (10^{-4} cm^{-1})	R value[a]
compd **2**	$g_3 = 2.295$	$A_3 = 125$	0.10
	$g_2 = 2.10$	$A_2 = 30$	
	$g_1 = 2.08$	$A_1 = 15$	
compd **3**	$g_3 = 2.09$	$A_3 = 145$	0.57
	$g_2 = 2.06$	$A_2 = 35$	
	$g_1 = 2.02$	$A_1 = 5$	
compd **4**	$g_3 = 2.23$	$A_3 = 110$	0.04
	$g_2 = 2.10$	$A_2 = 10$	
	$g_1 = 2.095$	$A_1 = 35$	
compd **5**	$g_3 = 2.23$	$A_3 = 95$	0.20
	$g_2 = 2.04$	$A_2 = 35$	
	$g_1 = 2.002$	$A_1 = 55$	
compd **6**	$g_3 = 2.25$	$A_3 = 95$	0.26
	$g_2 = 2.095$	$A_2 = 60$	
	$g_1 = 2.055$	$A_1 = 50$	
compd **7**	$g_3 = 2.225$	$A_3 = 125$	0.13
	$g_2 = 2.065$	$A_2 = 25$	
	$g_1 = 2.045$	$A_1 = 55$	
compd **8**	$g_3 = 2.200$	$A_3 = 90$	0.33
	$g_2 = 2.065$	$A_2 = 20$	
	$g_1 = 2.020$	$A_1 = 10$	

[a] $R = (g_2 - g_1)/(g_3 - g_2)$ with $g_3 > g_2 > g_1$.

EPR Spectroscopy. EPR spectroscopy has been used to evaluate the coordination environments of the Cu in **2**−**8** in frozen methanol, and the simulated EPR parameters of these complexes are summarized in Table 3. The frozen methanol solution EPR spectra of all of the Cu(II) complexes of **L2** and compound **3** display rhombic distortion (Figures S11 and S12). Spectral simulation data indicate that the coordination environments of the complexes are more consistent with distorted square pyramidal geometries than the trigonal bipyramidal geometries observed in the crystal structures of **4**−**6**. A similar shift toward square pyramidal geometries in solution has been observed by Masuda and co-workers for several related pyridine complexes.[13b,d] Interestingly, Micera and co-workers[44] recently reported that $[Cu(bpy)_2OH]^+$ in either frozen H_2O or H_2O(40%)−EtOH(60%) exhibits EPR spectra consistent with coordination environments intermediate between square pyramidal and trigonal bipyramidal. Simulation of the mixed solvent spectrum indicated considerable rhombic distortion of the coordination environment in $[Cu(bpy)_2OH]^+$, with $g_3 = 2.205$, $g_2 = 2.110$, and $g_1 = 2.100$, $A_3 = 130 \times 10^{-4}$ cm^{-1}, $A_2 = 25 \times 10^{-4}$ cm^{-1}, and $A_1 = 50 \times 10^{-4}$ cm^{-1}, and the calculated R value of 0.10. Hathaway et al.[45] have shown that R values greater than 1 indicate the ground state is d_{z^2}, and those less than 1 indicate a $d_{x^2-y^2}$ ground state.

The g values and A values of **2** at 77 K resemble other Cu(II) complexes with $d_{x^2-y^2}$ ground states, suggesting a distorted square pyramidal structure. Interestingly, the related $[Cu(bppa)]^+$ ion appears to have axial symmetry and displays a larger Cu hyperfine coupling constant[23b] compared to **2**; however, the Cu hyperfine coupling constants of both five-coordinate complexes are smaller than the values reported for square planar complexes such as $[Cu(bpba)MeOH]^{2+}$.[13d] Compounds **4**−**6** have more distorted coordination environments based on their respective g, A, and R values. As with compound **2**, the coordination environments of **4**−**6** appear to be closer to square pyramidal than trigonal bipyramidal, as reflected in their R values.[44] The frozen solution EPR spectra of **4**−**6**, therefore, suggest that the weak intermolecular interactions observed in the crystal structures of **4**−**6** may contribute to the stabilization of the observed distorted trigonal bipyramidal geometries.

The coordination geometries and ground-state configurations of the hydroperoxo− and *tert*-butylperoxo−Cu(II) complexes, **7** and **8**, respectively, also have been examined by low-temperature (77 K) EPR spectroscopy. The frozen MeOH solution spectra of **7** and **8** are very similar to the spectra of **2** and **4**, and on the basis of their simulated spectra, the g and A values are consistent with $d_{x^2-y^2}$ ground states and rhombic distorted structures and differ from those reported for the square planar $[Cu(bpba)OOH]^+$ complex.[13d] Also, the resulting R values are 0.13 and 0.33 for **7** and **8**, respectively, indicating the coordination environment in both complexes is nearly square pyramidal and different from the trigonal bipyramidal geometry reported for $[Cu(bppa)OOH]^+$ [12] and related pyridine derivatives in methanol and acetonitrile.[13b]

Electrochemistry. The electrochemical properties of **2**−**6** were evaluated by cyclic voltammetry. The redox behavior of **5** and **6** were found to be irreversible in methanol and acetonitrile unlike $[Cu(bppa)N_3]^+$,[23] $Cu(bpga)N_3$, and $Cu(bpaa)N_3$[13b] which are reported to display reversible one-electron oxidation−reduction in acetonitrile. The redox behavior of compounds **2**−**4** on the other hand is quasi-reversible in acetonitrile. The $E_{1/2}$ value of **2** is −150 mV versus Ag/AgCl compared to −110 mV observed for the tmima analogue, compound **3**. The related $[Cu(tpa)](ClO_4)_2$ and $[Cu(bppa)](ClO_4)$ complexes are reported to display quasi-reversible one-electron oxidation−reduction in acetonitrile with $E_{1/2}$ values of −85 [8c] and −135 mV[23d] versus Ag/AgCl, respectively.

Compound **4** displays a single quasi-reversible redox wave at −160 mV versus Ag/AgCl compared to −410 mV reported for the $[Cu(tmima)Cl]^+$ versus Ag/AgCl.[27a] The nearly 250 mV difference in redox potentials between **4** and $[Cu(tmima)Cl]^+$ is consistent with the electron-withdrawing nature of the pivaloamide pendants on the **L2** ligand.[29] $[Cu(tpa)Cl]^+$ and $[Cu(bppa)Cl]^+$ on the other hand display quasi-reversible redox waves at −615 and −48 mV versus Ag/AgCl,[23a] resulting in a 570 mV difference between the redox processes. A comparison of the changes in the Cu(II)/Cu(I) redox potentials for the amide forms of tmima, **L2**, relative to those of the related pyridine ligand, bppa, suggests the amide pendants on the pyridine chelate exert a greater electron-withdrawing effect.

Reactivity Studies of Compounds 2 and 3 with Peroxides. As mentioned earlier, many mononuclear copper proteins contain at least two coordinated histidine ligands in their active sites, and a growing number of copper proteins are thought to generate peroxo intermediates during key

(44) Garribba, E.; Micera, G.; Sanna, D.; Strinna-Erre, L. *Inorg. Chim. Acta* **2000**, *299*, 253−261.
(45) (a) Hathaway, B. J.; Billing, D. E. *Coord. Chem. Rev.* **1970**, *5*, 1. (b) Hathaway, B. J.; Duggan, M.; Murphy, A.; Mullane, J.; Power, C.; Walsh, A.; Walsh, B. *Coord. Chem. Rev.* **1981**, *36*, 267−324.

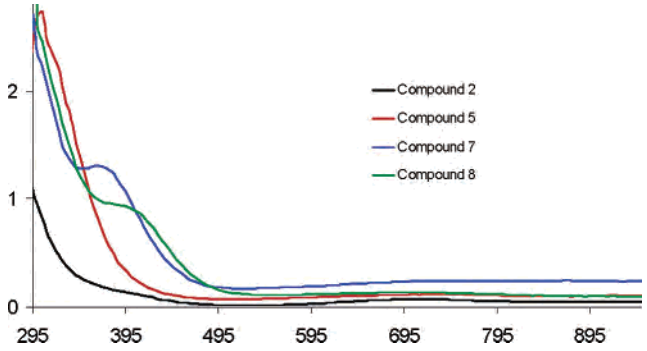

Figure 6. UV−visible spectra of **2** (1 mM), **5**, and peroxo species generated by the addition of alkyl and hydroperoxides to **5** in methanol at −40 °C.

biochemical pathways. Therefore, it is surprising that there are so few examples of mononuclear Cu−peroxo complexes containing imidazole ligands. In fact, to date there has been only one report of a spectroscopically detected Cu(II)−peroxo complex containing an imidazole ligand.[15] To probe the effect of imidazole coordination on the formation and stability of Cu(II)−peroxo species, we have examined the reactivity of **2** and **3** in the presence of base and H_2O_2 or in the presence of base and *tert*-butylperoxide.

Cu(II)−OH[8h] and Cu(II)−(H)OMe[13d] complexes have been used effectively in ligand exchange reactions with peroxides to form Cu−peroxo species. Similarly, Cu(II)−OH complexes of **L2** and tmima were employed in this study to probe peroxide coordination. The [Cu(**L2**)OH]$^+$ species, **5**, was prepared in situ from **2** and KOH and used to generate the Cu(II)−peroxo species **7** and **8**. Identical reaction conditions were employed to generate [Cu(tmima)OH]$^+$, which in turn was reacted further with H_2O_2 as discussed below.

The UV−visible spectrum of compound **2** (1 mM) in methanol displays a band at 415 nm ($\epsilon \approx 100$ M^{-1} cm^{-1}) and a weak d−d transition at 725 nm ($\epsilon \approx 70$ M^{-1} cm^{-1}) (Figure 6). The addition of 1 equiv of KOH to the methanol solution of **2** results in the rapid formation of a band near 315 nm with an extinction coefficient ϵ of 2375 M^{-1} cm^{-1}, which is similar to the spectrum of compound **5** in methanol. [Cu(**L2**)OH]$^+$ and [Cu(**L2**)OCH$_3$]$^+$ were detected in the ESI mass spectrum of the reaction mixture (Figure S13). The addition of 10 equiv[13,16] of 30% or 3% aqueous H_2O_2 to the mixture resulted in an immediate color change of the solution from green to yellow, concomitant with the appearance of a d−d band at 780 nm ($\epsilon = 240$ M^{-1} cm^{-1}) and a band in the UV region centered at 365 nm ($\epsilon = 1300$ M^{-1} cm^{-1}), assigned to a hydroperoxo $\pi^*_\sigma \rightarrow$ Cu LMCT transition.[11] The position and intensities of LMCT bands in Cu(II)−OOH complexes are very sensitive to the coordination environment of the Cu[11−17] and the solvent medium.[46] For the known Cu(II)−OOH complexes,[11−19] the five-coordinate complexes display hydroperoxo $\pi^*_\sigma \rightarrow$ Cu LMCT transitions at slightly longer wavelengths compared to the square planar complex, [Cu(bpba)OOH]$^+$, which exhibits an intense band at 350 nm ($\epsilon = 3400$ M^{-1} cm^{-1}).[13d] The LMCT (HOO$^- \rightarrow$ Cu(II)) band for **7** occurs at 365 nm and is less intense than the transition in [Cu(bpba)OOH]$^+$ but more intense than the related LMCT band observed for [Cu(bppa)OOH]$^+$,[12] which is observed at 390 nm ($\epsilon = 630$ M^{-1} cm^{-1}) in methanol and 380 nm ($\epsilon = 890$ M^{-1} cm^{-1}) in acetonitrile. The position of the band for **7** is more similar to the LMCT transitions reported for the carboxylate derivatives Cu(bpga)OOH (359 nm ($\epsilon = 890$ M^{-1} cm^{-1})) and Cu(bpaa)OOH (358 nm ($\epsilon = 300$ M^{-1} cm^{-1})) in methanol[13b] and the 357 nm value reported for the square pyramidal [Cu(N$_3$S-type)OOH]$^+$ complex.[17] Another five-coordinate square pyramidal complex, [Cu$_2$(XYL-O-)OOH]$^+$, which has a bridging hydroperoxo ligand, displays a LMCT transition at 395 nm.[8h,20] Finally, the addition of excess aqueous *tert*-butylperoxide (70%) to a methanol solution of **5** produces a LMCT band at 395 nm ($\epsilon = 950$ M^{-1} cm^{-1}), indicative of the formation of a *tert*-butylperoxo species.[11] A more thorough characterization of this complex is in progress.

To assess whether the amide pendants of **L2** are involved in stabilizing the peroxo adducts of **2** (e.g., **7** and **8**), the reactivity of [Cu(tmima)](ClO$_4$)$_2$ (**3**) was examined with H_2O_2 in the presence of base under the same reaction conditions. The tmima ligand lacks hydrogen-bonding amide pendants and likely coordinates to Cu(II) in a manner similar to **L2** and other tmima derivatives.[27] The addition of 1 equiv of KOH to a methanol solution containing **3** (1 mM) resulted in the formation of a OH$^- \rightarrow$ Cu(II) LMCT band at 315 nm ($\epsilon = 3750$ M^{-1} cm^{-1}) attributed to the [Cu(tmima)OH]$^+$ complex (Figure S14). Formation of [Cu(tmima)OH]$^+$ and [Cu(tmima)OCH$_3$]$^+$ in the reaction mixture was verified by ESI-MS (Figure S15). Further addition of 10 equiv of H_2O_2 at −40 °C produced no discernible hydroperoxo $\pi^*_\sigma \rightarrow$ Cu LMCT transition between 350 and 380 nm, as observed in the reaction with **5**. In fact, after the addition of H_2O_2, the original spectrum of **3** was regenerated, suggesting the hydroperoxo species, if formed, is not stable enough when coordinated to [Cu(tmima)]$^{2+}$ to be detected at this temperature. Masuda and co-workers observe a decrease in stability of the square planar [Cu(bpba)OOH]$^+$ complex at −78 °C in acetone compared to the trigonal bipyamidal [Cu(tpa)-OOH]$^+$ species and the significantly more stable [Cu(bppa)-OOH]$^+$ species.[13d] This observation suggests the amide pendants of **L2** in **7** are indeed hydrogen-bonding to the coordinated hydroperoxo ligand, which contributes to a greater thermodynamic stability of this species in solution.

The reactivity of **3** in the presence of base with H_2O_2 was examined further using EPR spectroscopy. The addition of 1 equiv of KOH to a methanol solution of **3** produced a new signal attributed to the [Cu(tmima)OH]$^+$ complex (Figure S16). The addition of 10 equiv of H_2O_2 to this solution, followed by its immediate freezing to 77 K, produced an EPR signal virtually identical to that of compound **3** (Figure S16). Similar results are obtained when excess ^{t}BuOOH is added to a solution of [Cu(tmima)OH]$^+$ in methanol. Overall, the results from the EPR study agree well with the UV−vis study described previously and support the conclusion that [Cu(tmima]$^{2+}$ does not stabilize a hydroperoxo (or ^{t}BuOO$^-$)

(46) Prins, L. J.; Reinhoudt, D. N.; Timmerman, P. *Angew. Chem., Int. Ed.* **2001**, *40*, 2383−2426.

Table 4. Summary of Resonance Raman ν(O−O) Vibrations for Mononuclear Cu(II)−OOH Complexes

compds	$\nu(^{16}O-^{16}O)$ cm^{-1}	ref
$[Cu_2(Py_2SSPy_2)(OOH)_2]^{2+}$	822,[a] 836[a]	14
$[Cu(bpba)OOH]^+$	834[a]	13d
$[Cu(HB(3\text{-}^tBu\text{-}5\text{-}^iPrpz)_3)OOH]^+$	843[b]	11
$[Cu(TPA)OOH]^+$	847[a]	13c
Cu(bpaa)OOH	848[c]	13b
$[Cu(pmed)OOH]^+$	848[a]	13a
$Cu_2(bdpi)OOH$	848[c]	15
$[Cu(TEPA)OOH]^+$	851[c]	16
$[Cu(paedp)OOH]^+$	853[a]	13a
$[Cu(L2)OOH]^+$	854[c]	this work
Cu(bpga)OOH	854[c]	13b
$[Cu(bppa)OOH]^+$	856,[a] 863[c]	13c
[Cu(N3SL1)OOH]+	881[a]	17

[a] In acetonitrile. [b] Solid. [c] In methanol.

species under the same reaction conditions employed to produce **7** (or **8**).

Finally, the formation of the [Cu(**L2**)OOH]$^+$ species under similar conditions used in the UV−vis and EPR studies was also demonstrated by ESI-mass spectrometry and resonance Raman spectroscopy. The addition of H_2O_2 to a methanol solution containing equal quantities of KOH and **2** at −40 °C produced a yellow solution of **7** that was analyzed immediately by ESI-MS and exhibited a parent mass ion at *m*/*z* 593.4. The ion cluster had the appropriate mass and theoretical isotopic distribution pattern predicted for [Cu(**L2**)OOH]$^+$ (Figure S17). It is important to note that under identical conditions, the reaction of H_2O_2 and $[Cu(tmima)]^{2+}$ in the presence of base did not produce a signal attributable to $[Cu(tmima)OOH]^+$. Rather, the only species detected in the mass spectrum was the parent mass ion of $[Cu(tmima)OCH_3]^+$ (Figure S15).

The yellow solution of **7** also was analyzed by resonance Raman spectroscopy (rRs). As with [Cu(bppa)OOH]$^+$ and other reported Cu−OOH complexes (Table 4), a resonance-enhanced vibration of the coordinated hydroperoxo anion was observed. Excitation into the tail of the 365 nm charge-transfer transition at −100 °C (laser excitation wavelength at 488.0 nm) revealed a resonance-enhanced vibration at 854 cm^{-1} that shifted to 808 cm^{-1} ($\Delta\nu$ = 46 cm^{-1}) when ^{18}O-labeled hydrogen peroxide was added (Figure S18). The frequency of the ν(O−O) band as well as its shift to a lower energy upon ^{18}O exchange is diagnostic of the formation of an end-on Cu(II)−OOH complex and similar to values reported previously for related complexes (Table 4).[11−17] The ν(O−O) frequency of **7** is lower in energy compared to that of [Cu(bppa)OOH]$^+$ (863 cm^{-1}) and identical to the value reported for Cu(bpga)OOH, which also displays a $\Delta\nu$ = 46 cm^{-1} shift upon the addition of ^{18}O-labeled hydrogen peroxide.[13b] In addition, the ν(O−O) frequency of **7** is higher than the value (834 cm^{-1}) reported for the square planar [Cu(bpba)OOH]$^+$ complex.[13d] Therefore, on the basis of the resonance Raman results, and the additional spectral data described above, compound **5** readily reacts with hydrogen peroxide at −40 °C to form a new Cu(II)−OOH species (**7**) that is more thermodynamically stable than the related species formed from compound **3** but less stable compared to [Cu(bppa)OOH]$^+$ reported by Masuda and co-workers.[12] Differences in the stability of Cu(II)−OOH species of **L2** and tmima in methanol may be attributed to the hydrogen-bonding properties of the amide pendants on **L2**.

Summary and Conclusions

The structure and properties of a new amide functionalized polyimidazole ligand and several mononuclear Cu(II) complexes containing different axially coordinated anion ligands (e.g., Cl$^-$, OH$^-$, N_3^-, HOO$^-$, and ^{t}BuOO$^-$) have been examined. Data from different physical measurements clearly show that **L2** when complexed to Cu(II) provides sufficient steric bulk to prevent formation of multimetallic complexes both in solution and in the solid state. The structures and properties of these anion complexes resemble those reported previously for related tmima derivatives[27] and pyridine complexes.[23] Compounds **4**−**6** have slightly distorted trigonal bipyramidal geometries in the solid state, whereas complexes of the related bppa ligand display more distorted coordination geometries. The N−H···X hydrogen bonding in the Cu−bppa complexes is stronger than in the Cu−**L2** complexes, which most likely contributes to the larger distortion of the Cu−bppa coordination environments. Nevertheless, the crystal structures of **4**−**6** clearly show that the amide pendants of **L2** form weak to moderately strong hydrogen bonds with different axially coordinated anion ligands, as reflected in the N···X separations and N−H···X angles. Similarly, hydrogen bonding involving **L2** is relevant to the observed stability of the hydroperoxo anion proposed for **7** in solution and may explain the difference in reactivity of **3** with H_2O_2, which lacks hydrogen-bonding amide pendants.

A comparison of the ligating ability and hydrogen-bonding properties of related Cu(II) complexes of bppa and **L2** yields two notable differences between the ligands. First, the Cu−N(Im) distances on average are shorter than the respective Cu−N(py) distances. This result is consistent with a stronger interaction between Cu and imidazole compared to pyridine, which also has been reported elsewhere.[27] In addition, the Cu−X (X = Cl$^-$, OH$^-$, or N_3^-) bonds in **4**−**6** are slightly longer than those reported for [Cu(bppa)X]$^+$ complexes,[23] which appears to be related to the longer Cu−N(amine) bonds of bppa compared to **L2**. The second difference between the ligands is the strength of the intramolecular hydrogen bonds, which are collectively stronger in bppa complexes compared to to the bonds in **4**−**6**. These results indicate that the anion ligands coordinated in **4**−**6** are more weakly bonded compared to related Cu−bppa complexes. This latter observation may explain why we are unable to detect the formation of [Cu(tmima)OOH]$^+$ under the same conditions employed to generate [Cu(**L2**)OOH]$^+$.

On the basis of the analysis of the spectroscopic data of compound **7** and crystal structures of **4**−**6**, the formation and thermodynamic stability of the mononuclear Cu(II)−OOH species, **7**, are clearly related to the steric bulk and hydrogen-bonding properties of the **L2** ligand. Formation of the yellow [Cu(**L2**)OOH]$^+$ ion was established by ESI-MS and further substantiated by the observation of a hydroperoxo $\pi^*_\sigma \rightarrow$ Cu LMCT transition at 365 nm (ϵ = 1300 M^{-1} cm^{-1}) in the UV−vis spectrum of **7** in methanol

at −40 °C. $[Cu(tmima)OOH]^+$ on the other hand was not detected by either ESI-MS or UV−vis spectroscopy when a methanol solution of $[Cu(tmima)OH]^+$ was treated with H_2O_2.

The formation of $[Cu(\mathbf{L2})OOH]^+$ also was observed by EPR spectroscopy. There was a rapid change in the EPR spectrum of **5** after the addition of H_2O_2. The 77 K EPR spectrum of **7** is consistent with a mononuclear species having a $d_{x^2-y^2}$ ground state, as observed for the other structurally characterized $[Cu(\mathbf{L2})X]^+$ species in this study. Under the same reaction conditions used to generate **7**, addition of excess H_2O_2 resulted in the disappearance of the EPR spectrum of $[Cu(tmima)OH]^+$ and the re-formation of the original spectrum of $[Cu(tmima)]^{2+}$. This result further substantiates our conclusion that the $[Cu(tmima)OOH]^+$ species, if formed, is not stable enough to be detected under the same reaction conditions employed for compound **7**. The spectroscopic properties of compound **8** also were studied using UV−vis and EPR. In methanol at −40 °C, **8** displays a band at 395 nm (ϵ = 950 M^{-1} cm^{-1}) assigned to an alkylperoxo $\pi^*_\sigma \rightarrow$ Cu LMCT transition,[11] and the 77 K EPR spectrum is similar to the spectrum of **7** and consistent with a $d_{x^2-y^2}$ ground state.

The most compelling evidence for the formation of a new Cu(II)−OOH species containing **L2** comes from the analysis of the resonance Raman data of **7** in methanol at −100 °C, which shows a resonance-enhanced ν(O−O) vibration at 854 cm^{-1} that shifted to 808 cm^{-1} ($\Delta\nu$ = 46 cm^{-1}) upon the addition of ^{18}O-labeled hydrogen peroxide. The region of the vibration as well as the magnitude of its shift upon ^{18}O exchange is consistent with the behavior of other proposed end-on hydroperoxo−Cu(II) species.

This study demonstrates the utility of amide functionalized imidazole tripods in stabilizing biologically relevant copper−hydroxo and −peroxo species through a combination of ligand steric effects and intramolecular hydrogen bonding. The enhanced thermal and chemical stability of the species, compared to their tmima analogues, is attributed to the hydrogen-bonding properties of the **L2** amide pendants. Finally, the flexibility of the synthetic protocol described herein to prepare **L2**, and related species,[47] should allow us to prepare a new class of amide functionalized imidazole ligands for future biomimetic structure−activity studies.

Acknowledgment. We gratefully acknowledge the support of the National Science Foundation (Grant CHE-0328406) and the Kentucky Science and Engineering Foundation (Grant KSEF-275-RDE−003). M.S.M. thanks the Kentucky Research Challenge Trust Fund for the upgrade of our X-ray facilities. We would like to thank Prof. Craig Grapperhaus for helpful EPR discussions. Dr. William Pierce, Jr., and Ned Smith at the University of Louisville Biomolecular Mass Spectrometry Laboratory provided assistance in obtaining ESI and HRMS data. Funding for the resonance Raman instrumentation was provided by the University of Cincinnati.

Supporting Information Available: Detailed crystallographic refinements for compounds **4**−**6**; ^{1}H and ^{13}C NMR spectra of **1** and **L2** (all regions) (Figures S1−S5); representation of intermolecular interactions for compounds **L2** and **4**−**6** (Figures S6−S10); experimental and simulated X-band EPR spectra of **2**−**8** (Figures S11 and S12); UV−vis (Figure S14) and EPR (Figure S16) spectra of complex **3** upon addition of H_2O_2; ESI-MS spectrum of Cu(II) complexes of **L2** (Figure S13), tmima (Figure S15), and **7** (Figure S17); resonance Raman spectra of **7** (Figure S18); crystallographic data, structure refinement details, atomic coordinates, interatomic distances and angles, torsion angles, anisotropic displacement parameters, and hydrogen parameters in CIF format. This material is available free of charge via the Internet at http://pubs.acs.org.

IC051280S

(47) Cheruzel, L. E.; Mashuta, M. S.; Buchanan, R. M. Manuscript to be submitted for publication.